**Laser trapping and manipulation of micro/nano-objects on polymer substrates***

YIN Yue, DOU Lin, SHEN Tianci, LIU Jiatong, GU Fuxing

School of Optical-Electrical and Computer Engineering, University of Shanghai for Science and Technology, Shanghai 200093, China

**Abstract**

Polymer substrates overcome the limitations of rigid planar substrates in spatial deformation scenarios and can be combined with photolithography to fabricate complex, three-dimensional, irregular polymer structures. The photothermal-shock tweezer is a laser trapping technique based on the photothermal shock effect. The photothermal-shock tweezer utilizes pulsed laser-induced transient photothermal shock to generate a micro-newton-scale thermomechanical strain gradient force, enabling the trapping and manipulation of micro/nano-objects at solid interfaces. Integrating this technique with polymer substrates can meet the demands of new application scenarios. In this work, polymethyl methacrylate (PMMA) and negative photoresist (SU-8) are commonly employed as polymer substrates, on which $SiO_2$ nanofilms are prepared using the sol-gel method. This method effectively mitigates thermal damage caused by photothermal shock effects, enabling laser trapping and manipulation of micro/nano-objects. The $SiO_2$ nanofilms, characterized by low thermal conductivity, effectively inhibit heat transfer. The nanofilm fabrication technique utilized in this study enables the synthesis of large-area $SiO_2$ nanofilms with large-area coverage, low surface roughness ($R_q$ ~ 320 pm), and uniform thickness, making them broadly applicable to flexible polymer substrates and irregular structures. Direct contact between the polymer layer and micro/nano-objects during manipulation of the photothermal shock tweezers can induce irreversible substrate degradation due to transient photothermal shock effects. Experimental results demonstrate that depositing an $SiO_2$ nanofilm thicker than 110 nm on the polymer substrate can significantly enhance thermal insulation and protection, effectively mitigating laser-induced damage under typical optical manipulation conditions. Additionally, by analyzing the temperature field distribution of the gold nanosheet, PMMA substrate, and $SiO_2$ nanofilm during a single photothermal shock trapping of a gold nanosheet, it is found that the $SiO_2$ nanofilm can reduce the PMMA surface temperature by at least 111 ℃ and delay the time for PMMA to reach its peak temperature by 13.2 ns compared with the gold nanosheet. The experimental results expand the environmental medium for laser trapping of objects,

---

* The paper is an English translated version of the original Chinese paper published in Acta Physica Sinica. Please cite the paper as: **YIN Yue, DOU Lin, SHEN Tianci, LIU Jiatong, GU Fuxing**. **Laser trapping and manipulation of micro/nano-objects on polymer substrates**, Acta Phys. Sin., 2025, 74(8): 088703. doi: 10.7498/aps.74.20241654

providing new possibilities for applications in micro/nano-manipulation, micro/nanorobotics, and micro/nano-optoelectronic devices.

Keywords: laser trapping, polymer surface, sol-gel method, photothermal-shock tweezer

**PACS**：87.80.Cc, 68.47.Mn, 81.15.–z, 42.50.Wk

**doi:** 10.7498/aps.74.20241654

**cstr:** 32037.14.aps.74.20241654

## 1. Introduction

Laser trapping is a powerful tool for non-contact manipulation of micro/nano-objects[1–7]. Based on the principle of forming an optical gradient force trap via photon momentum, the micro/nanoscale optical force (~ pN) generated by conventional optical tweezers cannot overcome the van der Waals adhesion force (~ μN) at solid interfaces, so it is usually used in vacuum/air and liquid environments[8]. The photothermal-shock tweezer, invented by Gu Fuxing's research group, has enabled the trapping of micro/nano-objects (such as metal and few-layer graphene) at solid interfaces (dry solid, solid-liquid mixing). When integrated with the closed-loop control system[9] based on deep-learning image feedback, the photothermal-shock tweezer further achieves the high-precision and intelligent control of micro/nano-object motion[10–14]. The core principle of the photothermal-shock tweezer lies in employing a pulsed laser to locally induce the photothermal shock effect inside the micro/nano-object, thereby triggering instantaneous thermal expansion and generating a micro-newton-scale thermomechanical strain gradient force. This force overcomes the frictional constraints of the solid interface, driving the object toward the center of the laser spot. Under Gaussian-beam illumination, the object can continue to move toward the beam center and is eventually trapped.

At present, the substrates used in photothermal-shock tweezers are mainly inorganic rigid materials ($SiO_2$, $MgF_2$, $Al_2O_3$). However, flexible optical substrates are not constrained by the rigid physical state of traditional materials, and their bendable and stretchable characteristics greatly broaden the application scenarios of micro/nano optical manipulation[15]. Polymer materials, such as polymethylmethacrylate (PMMA) and polydimethylsiloxane (PDMS), possess good mechanical flexibility, optical transparency, and stability, making them the ideal candidates for flexible optical substrates. Nevertheless, the low thermal stability and high thermal expansion coefficient of polymers mean that the transient photothermal shock effects generated by the photothermal-shock tweezers can induce irreversible damage (thermal melting, permanent deformation) [10,13,16], thereby restricting their application on polymer substrates. In addition, organic photoresists (negative photoresist SU-8 series and positive

photoresist S18 series) exhibit good structural integrity and moulding stability, and can be processed into complex three-dimensional irregular structures via two-photon polymerization (TPP). These photoresists have been widely employed in the precision manufacturing of micro/nano optoelectronic devices and micromechanical structures[17–19]. However, their inherently low thermal conductivity still poses certain limitations for applying the photothermal-shock tweezers on their surfaces.

The $SiO_2$ nanofilm has low thermal conductivity and can effectively block heat transfer, thereby enhancing the thermal resistance of the polymer substrates when integrated with $SiO_2$ amorphous nanomaterial [20]. However, to achieve large-area, low-surface-roughness, and uniform-thickness $SiO_2$ nanofilms on polymer substrates, it is crucial to select an appropriate deposition technique. Traditional deposition methods include chemical vapor deposition (CVD), physical vapor deposition (PVD) through evaporation or sputtering, and plasma-enhanced chemical vapor deposition (PECVD)[21]. Among them, CVD and PVD typically require high deposition temperature, which can induce thermal degradation of polymer substrates, leading to deformation or cracking. Although PECVD can be conducted at low temperature, the rapid plasma deposition process will increase the surface roughness ($R_q$ > 500 pm). The significant optical loss associated with these deposition processes hinders the effective integration of $SiO_2$ nanofilms with polymer substrates. In contrast, the sol-gel method enables large-area fabrication of $SiO_2$ nanofilms at room temperature with a controllable deposition process. The resulting $SiO_2$ nanofilm exhibits low surface roughness ($R_q$ < 500 pm) and uniform thickness. Moreover, $SiO_2$ nanofilms possess a high elastic deformation limit, allowing conformal deposition on both planar and non-planar substrates. This provides greater versatility and broader application potential for integrating amorphous nanomaterials with polymer substrates [22,23].

In this paper, $SiO_2$ nanofilms were fabricated on polymer substrates using the sol-gel method, which effectively mitigates the thermal damage induced by photothermal shock tweezers, thereby enabling stable laser trapping and manipulation of micro/nano-objects on polymer substrates. Large area $SiO_2$ nanofilms with low surface roughness ($R_q$ ~ 320 pm) and uniform thickness were fabricated on PMMA and SU-8 polymer substrates at room temperature. Experimental results revealed that $SiO_2$ nanofilms with a thickness exceeding 110 nm effectively suppressed the softening, expansion, and surface damage of the polymer substrate caused by the photothermal shock effect under typical optical manipulation conditions. Theoretical analysis demonstrated that the $SiO_2$ nanofilm reduced the PMMA surface temperature by over 111 °C and introduced a 13.2 ns delay in reaching its peak temperature compared with the gold nanosheet. In addition, the experimental results are also applicable to the SU-8 polymer structure prepared by TPP technology.

## 2. Sample preparation

PMMA and SU-8 were selected as polymer substrates. In this study, PMMA powder was dissolved in anisole solution to prepare a 10% PMMA solution, and a 1.5 μm-thick PMMA film was fabricated on a $SiO_2$ substrate by spin coating. The three-dimensional microfabrication of SU-8 photoresist was performed using TPP technology. Specifically, the SU-8 photoresist was spin-coated onto the $SiO_2$ substrate, followed by pre-baking, exposure, post-baking, and development to obtain the desired SU-8 polymer structures. The $SiO_2$ sol-gel was synthesized by a sol-gel method, with hydrochloric acid as the catalyst. Tetraethyl orthosilicate and deionized water served as reactants, while anhydrous ethanol was used as the solvent. These components were mixed in specific proportions to form a homogeneous solution, which was sealed and agitated in a micro-vortex mixer at 2000 rad/min for 2 hours. The process yielded a stable $SiO_2$ sol-gel. Fig. 1(a) illustrates the schematic flow chart of the preparation of $SiO_2$ nanofilms on polymer substrates. First, the commercial fused silica substrates were ultrasonically cleaned in acetone, ethanol, and deionized water for 20 minutes each. Then, a PMMA or SU-8 polymer layer was deposited as required. Subsequently, the $SiO_2$ sol-gel was drop-cast onto the polymer layer and spin-coated at 6000 rad/min to form a uniform $SiO_2$ nanofilm. After coating, the sample was left to dry naturally for 15 minutes, followed by thermal treatment at 60 ℃ for 1 hour to ensure the organic solvent was completely volatilized.

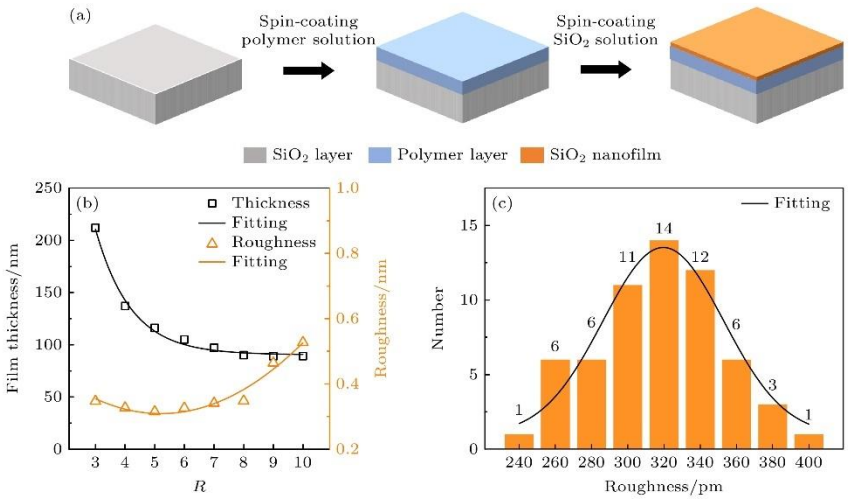


**Figure 1.** Preparation and surface characteristics of $SiO_2$ nanofilms: (a) Preparation process of $SiO_2$ nanofilms on polymer substrates; (b) variation of $SiO_2$ nanofilm thickness and surface roughness with *R* values; (c) histogram of surface roughness distribution of $SiO_2$ nanofilms under the condition of $R = 5$.

The deposition thickness and surface morphology of $SiO_2$ nanofilms significantly influence the thermal insulation performance and the trapping accuracy of the photothermal-shock tweezer. Therefore, by adjusting the volume ratio of ETOH to TEOS ($R = V_{ETOH}/V_{TEOS}$), we

prepared eight different $SiO_2$ sol-gel solutions with *R* values ranging from 3 to 10. The resulting sols were spin-coated onto a fused silica substrate to form $SiO_2$ nanofilms, dried for 15 min, and subsequently heated at 60 ℃ for 1 hour at constant temperature to complete the film preparation. The thickness and surface roughness of $SiO_2$ nanofilms were characterized multiple times using an atomic force microscope (AFM, Cypher S), and the results are presented in Fig. 1(b). The film thickness can be controlled by adjusting the *R* value, and the minimum thickness can be as low as 90 nm. It is noteworthy that the relationship between film thickness and *R* value is nonlinear: as R increases, the film thickness tends to saturate, whereas the surface roughness increases markedly, providing a practical reference for the subsequent selection of film thickness.

According to the results in Fig. 1(b), sixty $SiO_2$ nanofilm samples with a thickness of 115 nm were selected under the condition of $R = 5$ for surface roughness measurements. The scanning area was 5 μm × 5 μm, with all other parameters kept constant. The results, as shown in Fig. 1(c), indicate that the surface roughness of the $SiO_2$ nanofilms ranges from 240 to 400 pm, with a dominant distribution around (320 ± 10) pm. These results confirm that the $SiO_2$ nanofilms prepared via the sol-gel method exhibit superior surface flatness compared with commercial fused silica substrates ($R_q$ ~ 550 pm).

**3. Experimental result**

In this experiment, a 532 nm pulsed laser (repetition rate of 6000 Hz, pulse width of 8 ns) was used to capture and manipulate micro/nano-objects on a photothermal-shock tweezer platform. Due to the high peak energy of the pulsed laser, the photothermal effect induced by direct irradiation of the substrate surface was examined as the basis for subsequent polymer analyses. The focused spot was first scanned across the surface of a 1.5 μm thick PMMA substrate, with the following parameters: spot diameter $D_{spot}$ = 8.8 μm, average power $P_{ave}$ = 126 μW. As shown in the optical microscope image in Fig. 2(a), no visible damage was observed on the PMMA surface. However, AFM scanning revealed a series of distinct pits with varying depths along the path of the focused spot, as shown in Fig. 2(b) and (c). The pit width was approximately 200 nm, with depths ranging from 2 nm to 7 nm, indicating that the pulsed laser can directly induce irreversible thermal damage on the PMMA surface.

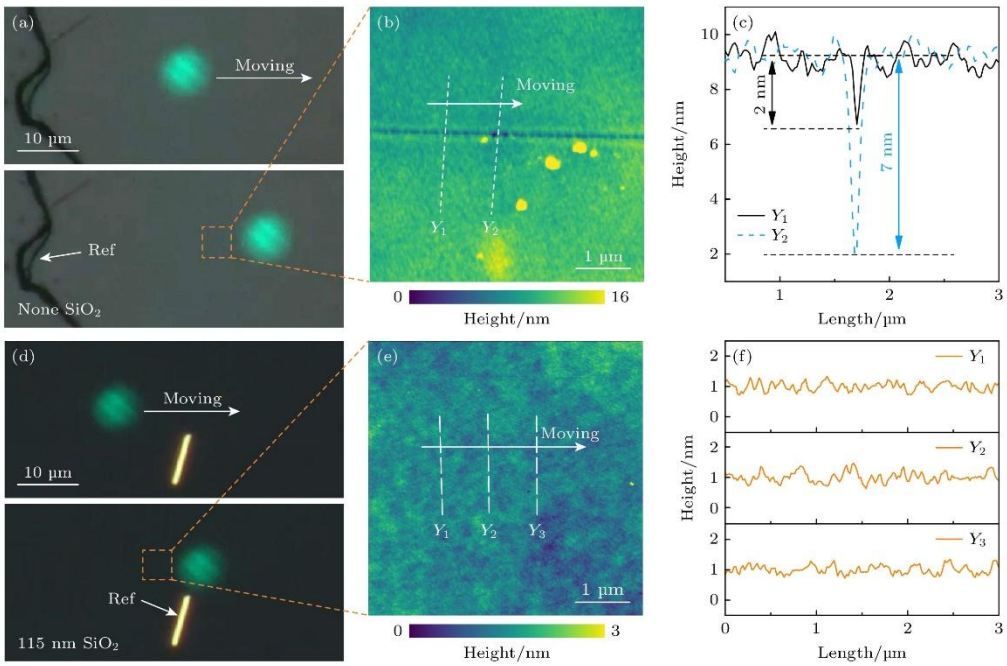


**Figure 2.** Comparison of motion traces on PMMA with/without $SiO_2$ nanofilms (the dashed parameter *Y* denotes the location of data measurement): (a)–(c) Optical micrographs and AFM scanning results of motion traces on PMMA without $SiO_2$ nanofilm; (d)–(f) optical micrographs and AFM scanning results of motion traces on PMMA with a 115 nm thick $SiO_2$ nanofilm.

Furthermore, to investigate the protective effect of the $SiO_2$ nanofilm, the same focused spot was scanned across the PMMA substrate coated with a 115 nm thick $SiO_2$ nanofilm (PMMA thickness: 1.5 μm), followed by surface analysis after laser irradiation. The optical micrographs in Fig. 2(d) and the AFM results in Fig. 2(e) and (f) demonstrate that the substrate surface remains undamaged, in sharp contrast to the thermal damage observed in Fig. 2(b). These results indicate that the 115 nm thick $SiO_2$ nanofilm provides an effective protective layer for the PMMA substrate.

To further examine the thermal insulation effect of $SiO_2$ nanofilm thickness on PMMA substrate, COMSOL software was employed to simulate the temperature field distribution of gold nanosheets, PMMA substrate, and $SiO_2$ nanofilm during a single photothermal shock of gold nanosheets. The maximum temperature distribution of each layer was first simulated when the gold nanosheet was in direct contact with the PMMA substrate, as shown in Fig. 3(a). When the gold nanosheet was actuated, its center temperature reached 272 ℃, significantly exceeding the softening temperature of PMMA (140 ℃), thereby causing irreversible damage to the PMMA substrate.

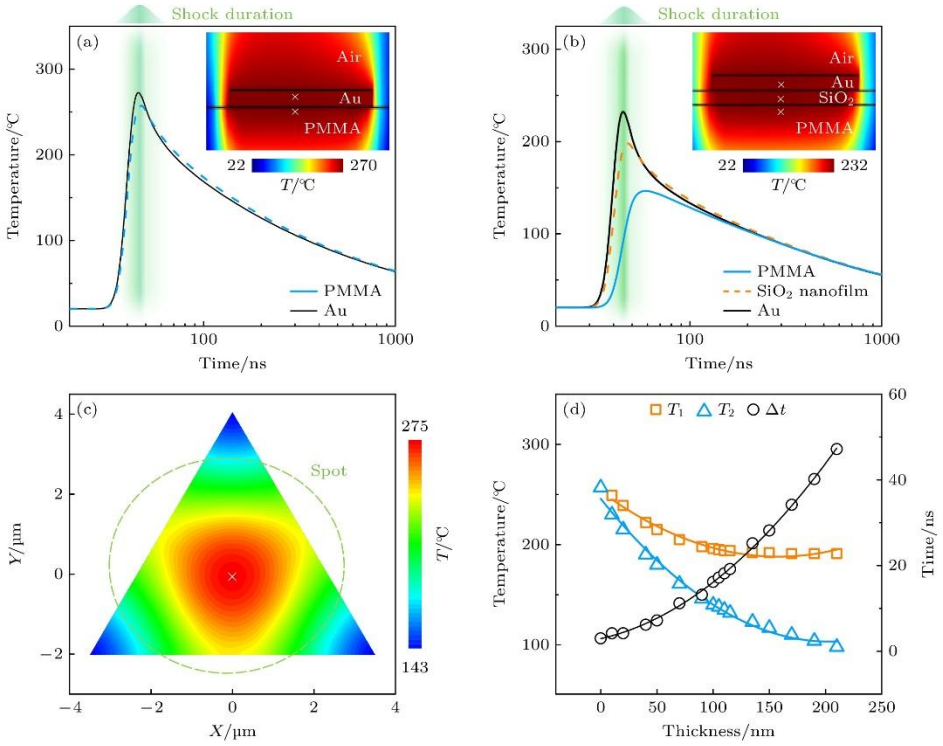


**Figure 3.** Simulation of the temperature field distribution across substrate layers during a single photothermal shock of gold nanosheets (the white crosshairs and the green dotted circles denote the object's center of mass and the light spots, respectively): Simulation of temperature distribution across substrate layers and surface peak temperature distribution during a single photothermal shock of a gold nanosheet on PMMA without $SiO_2$ nanofilms (a) and with a 90 nm thick $SiO_2$ nanofilm (b); (c) simulated temperature distribution on the surface of the gold nanosheet at a pulse duration of 44.8 ns; (d) relationship diagram between the $SiO_2$ nanofilm thickness and $T_1$, $T_2$, $\Delta t$, where $T_1$ represents the maximum surface temperature of the $SiO_2$ nanofilm, $T_2$ represents the maximum surface temperature of the PMMA, and $\Delta t$ represents the time delay.

Given that the minimum thickness of the $SiO_2$ nanofilm prepared by the sol-gel method in this study is approximately 90 nm, the maximum temperature distribution of each layer was simulated during a single photothermal shock of the gold nanosheet on the PMMA substrate with a 90 nm thick $SiO_2$ nanofilm. The results are shown in Fig. 3(b). It is evident that the presence of the $SiO_2$ nanofilm significantly lowers the surface temperature of PMMA and induces a 13.2 ns delay in the occurrence of its peak temperature compared with that of the gold nanosheet. The delay corresponds to the period during which the gold nanosheet undergoes its most rapid cooling. When the maximum surface temperature of PMMA reaches 146 ℃, it requires only 23 ns to decrease to 136 ℃, which is below the softening temperature of PMMA. However, because the maximum surface temperature of PMMA exceeds its softening temperature, thermal softening of the PMMA substrate may occur. Meanwhile, the

simulated temperature distribution on the surface of gold nanosheets at a pulse duration of 44.8 ns is shown in Fig. 3(c). Under Gaussian beam irradiation, the temperature distribution of the gold nanosheet exhibits a Gaussian profile, characterized by a maximum at the center and a gradual decrease toward the edges.

To determine the minimum thickness of $SiO_2$ nanofilm required to prevent thermal softening of the PMMA substrate, the thickness of $SiO_2$ nanofilm was varied while keeping the PMMA substrate thickness and laser spot parameters constant. The relationships of $T_1$ (the maximum surface temperature of $SiO_2$ nanofilm), $T_2$ (the maximum surface temperature of PMMA substrate), and $\Delta t$ (the time delay for PMMA substrate surface to reach its maximum temperature relative to that of gold nanosheets) with the $SiO_2$ nanofilm thickness are shown in Fig. 3(d). As $SiO_2$ nanofilm thickness increases, both $T_1$ and $T_2$ decrease, with $T_2$ exhibiting a more pronounced decline. Meanwhile, $\Delta t$ shows an upward trend, indicating that the $SiO_2$ nanofilm effectively suppresses heat conduction from the gold nanosheet to the PMMA substrate, thereby prolonging the heat transfer time. These results demonstrate that increasing the nanofilm thickness effectively reduces the maximum surface temperature of the PMMA substrate. When the $SiO_2$ nanofilm thickness increases from 90 nm to 110 nm, the magnitude of temperature reduction increases from 111 ℃ to 122 ℃.

To verify the protective capability of the $SiO_2$ nanofilm, experimental tests were conducted using nanofilms with a thickness of 90 nm ($R$ = 8) and 115 nm ($R$ = 5). In the experiment, a laser spot($D_{spot}$ = 7.6 μm, $P_{ave}$ = 105 μW) was employed to trap a regular triangular gold nanosheet with a side length of 7 μm and a thickness of 125 nm, which was actuated on a PMMA substrate coated with a 90 nm thick $SiO_2$ nanofilm. Fig. 4(a) presents an optical micrograph of gold nanosheet motion, showing that no visible damage occurred along its trajectory. To further examine potential substrate modification, AFM scans were performed along the trajectory, which revealed clear thermal damage features on the PMMA substrate surface caused by the gold nanosheet's actuation, as shown in Fig. 4(b) and (c). The damage features along the trajectory were characterized by depressions of approximately 3 nm at the center and at distances of 3 μm and 2.8 μm away from the center, while the surrounding regions exhibited protrusions with a maximum height of 8.3 nm. Considering that the surface temperature distribution of the gold nanosheet during actuation follows a Gaussian profile, with the highest temperature at the center and decreasing toward the periphery, and that the cooling time is very short, as indicated by previous simulations, the observed protrusions are attributed to the irreversible thermal expansion of PMMA in the central high-temperature region. In addition to the central damage feature along the gold nanosheet's motion trajectory, two lateral depressions were observed on either side. The distances of these lateral depressions from the central depression closely matched the distances from the nanosheet's center to its two corners. Therefore, these lateral depressions are attributed to polymer

retraction in the relatively low temperature regions beneath the three corners of the gold nanosheet. These results demonstrate that the 90 nm $SiO_2$ nanofilm is insufficient to fully protect the PMMA substrate from the photothermal effect, while further confirming that the $SiO_2$ nanofilm can accommodate slight deformations of the flexible polymer substrate without structural damage.

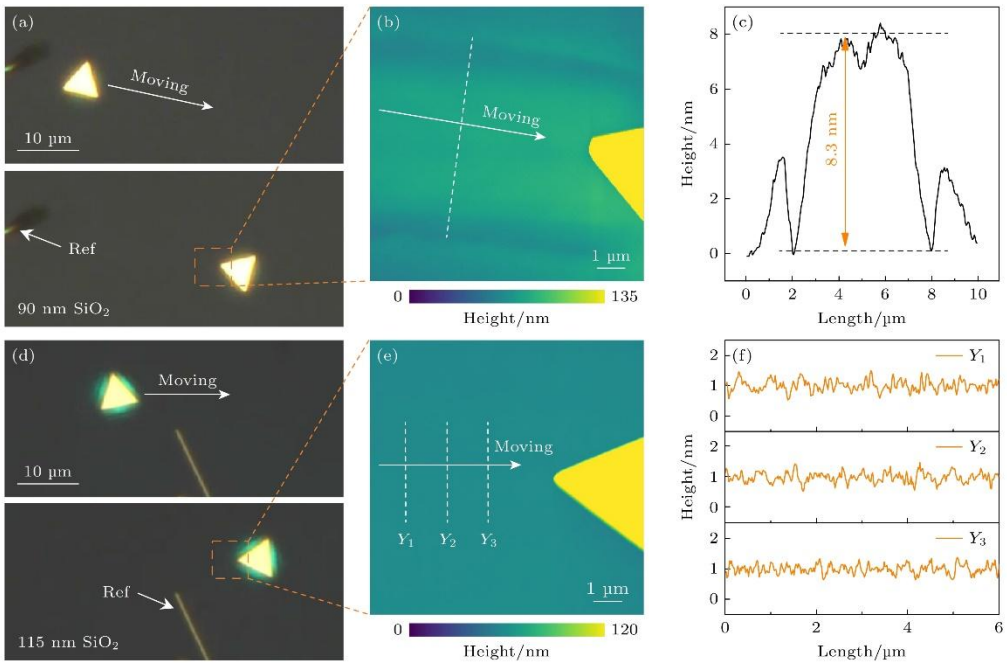


**Figure 4.** Comparison of motion traces of gold nanosheets on PMMA with $SiO_2$ nanofilms of different thicknesses (the dashed parameter *Y* denotes the location of data measurement): (a)–(c) Optical micrographs and AFM scanning results of motion traces of a gold nanosheet on PMMA with a 90 nm thick $SiO_2$ nanofilm; (d)–(f) optical micrographs and AFM scanning results of motion traces of a gold nanosheet on PMMA with a 115 nm thick $SiO_2$ nanofilm.

Furthermore, a laser spot with similar parameters ($D_{spot}$ = 7.8 μm, $P_{ave}$ = 98 μW) was employed to trap a regular triangular gold nanosheet (side length = 7.1 μm, thickness = 100 nm) and was actuated on a PMMA substrate coated with a 115 nm thick $SiO_2$ nanofilm. Fig. 4(d) shows the optical micrograph of the gold nanosheet's motion trajectory, from which it can be seen that no damage features occurred. Fig. 4(e) and (f) present AFM scans of the motion trajectory, revealing no detectable surface traces. These results indicate that, compared with the 90 nm $SiO_2$ nanofilm, the 115 nm $SiO_2$ nanofilm effectively suppresses thermally induced deformation of the PMMA substrate. This enhanced protective performance is consistent with the simulation results.

Both simulation and experiment confirm that a 115 nm thick $SiO_2$ nanofilm effectively protects the PMMA substrate from thermal damage when gold nanosheets are trapped and manipulated by photothermal-shock tweezers, thereby ensuring stable trapping and manipulation. Based on this conclusion, we further compared the surface roughness before

and after the motion trajectories of different gold nanostructures (gold nanowires and gold nanosheets) trapped under typical optical manipulation conditions, providing an in-depth analysis of the influence of laser trapping on the surface properties of the PMMA substrate with a 115 nm thick $SiO_2$ nanofilm. By calculating the surface roughness before ($R_1$) and after ($R_2$) trapping, the absolute change in surface roughness (ΔR) was obtained. As shown in Fig. 5(a), a statistical analysis of 12 gold nanostructures reveals that Δ$R$ ranged from 23 pm to 39 pm, indicating that the laser trapping process increases the surface roughness of the substrate along the motion path.

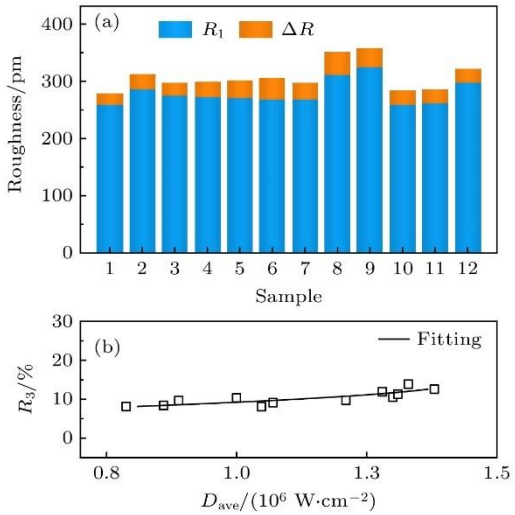


**Figure 5.** Comparison of surface roughness before and after the motion path of gold nanostructures: (a) Statistical data of $R_1$ and Δ$R$ for gold nanostructures; (b) relationship diagram between the average laser power density and the relative variation in the substrate surface roughness.

Due to the variations in shape and thickness among different gold nanostructures, different $D_{spot}$ and $P_{ave}$ values were required for trapping. Therefore, the average power density ($D_{ave}$) used for 12 samples was adopted as a unified reference parameter. As shown in Fig. 5(b), the relative change in substrate surface roughness ($R_3 = \Delta R/R_1$) increases with increasing $D_{ave}$, although the trend remains relatively moderate. Considering that AFM measurements provide sub-nanometer resolution, measurement deviations of less than 40 pm may occur. Given the small magnitude of roughness variation, the influence of increasing $D_{ave}$ on the morphology of the PMMA substrate with a 115 nm thick $SiO_2$ nanofilm can be regarded as negligible under typical optical manipulation conditions.

Building on the above results obtained with PMMA substrates, SU-8 was employed as an alternative polymer substrate to further verify the universality of the thermal protection provided by the 115 nm thick $SiO_2$ nanofilm. A laser spot ($D_{spot}$ = 8.7 μm, $P_{ave}$ = 135 μW) was used to trap a regular triangular gold nanosheet (side length = 7.2 μm, thickness = 310 nm),

which was moved on an SU-8 substrate without a $SiO_2$ nanofilm. As shown in the optical micrograph in Fig. 6(a) and the AFM topography in Fig. 6(b), the photothermal-shock tweezer induced pronounced traces on the SU-8 surface. When a 115 nm thick $SiO_2$ nanofilm was coated on the SU-8 substrate, a regular triangular gold nanosheet (side length = 7.1 μm, thickness = 100 nm) was trapped by a laser spot ($D_{spot}$ = 12.5 μm, $P_{ave}$ = 271 μW) and moved across the substrate surface. As shown in Fig. 6(c) and Fig. 6(d), no detectable surface damage was observed. The results confirm that the 115 nm thick $SiO_2$ nanofilm can effectively prevent the thermal damage of SU-8 polymer caused by laser trapping.

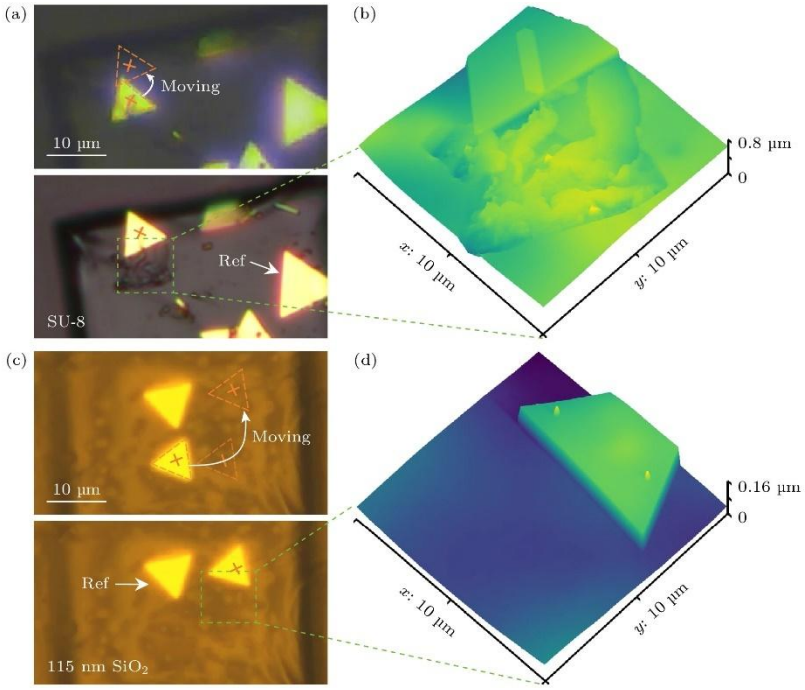


**Figure 6.** Comparison of motion traces of gold nanosheets on SU-8 with/without $SiO_2$ (The orange crosshair and the orange dashed triangle represent the centroid of the object and the gold nanosheet, respectively): (a), (b) Optical micrographs and AFM surface morphology of motion traces of a gold nanosheet on SU-8 without $SiO_2$ nanofilms; (c), (d) optical micrographs and AFM surface morphology of motion traces of a gold nanosheet on SU-8 with a 115 nm thick $SiO_2$ nanofilm.

## 4. Conclusion

In this study, $SiO_2$ nanofilms were prepared via the sol-gel method and employed as thermal insulation layers on a polymer substrate. The results demonstrate that $SiO_2$ nanofilms can effectively prevent thermal damage to the polymer substrate induced by the photothermal effect, thereby enabling non-destructive laser trapping and precise manipulation of micro/nano-objects using photothermal-shock tweezers. To verify this, the representative flexible material PMMA and the commonly used UV-curable photoresist SU-8 were employed as polymer substrates for three-dimensional microfabrication. Large-area $SiO_2$

nanofilms with low surface roughness and uniform thickness were deposited on the substrate surface via the sol-gel method, which can be carried out at room temperature. Compared with direct laser irradiation on polymer interfaces, $SiO_2$ nanofilms thicker than 110 nm provide excellent thermal insulation and protection under typical optical manipulation conditions. Theoretical calculations indicate that when a gold nanosheet reaches its peak temperature during laser trapping, the $SiO_2$ nanofilm not only delays thermal conduction to the PMMA surface but also reduces the PMMA surface temperature by at least 111 ℃. Moreover, as film thickness increases, the delay in thermal conduction is further extended, resulting in enhanced insulation against higher temperatures.

The experimental results demonstrate strong potential for integrating with a broader range of optical manipulation techniques at solid interfaces to achieve multidimensional, precise manipulation[8]. Furthermore, by combining the fabrication concept of $SiO_2$ nanofilms with polymer-based meta-surfaces and leveraging the unique properties of structured light (such as singular beams), the application scope of the photothermal-shock tweezers can be further expanded[6,24–26]. The proposed substrate fabrication method is applicable not only to non-biological flexible polymer substrates but also to irregular polymer structures fabricated by three-dimensional printing, thereby offering novel possibilities for applications in the fields of micro/nano manipulation[5,10–14], micro/nano robots[27–30], and micro/nano opto-electromechanical devices[19].

**References**

[1] Li N, Zhu X M, Li W Q, Fu Z H, Hu M Z, Hu H Z 2019 Front. Inform. Technol. Electron. Eng. 20 655

[2] Wang H C, Li Z P 2019 Acta Phys. Sin. 68 144101

[3] Han X, Chen X L, Xiong W, Kuang T F, Chen Z H, Peng M, Xiao G Z, Yang K Y, Luo H 2021 Chin. J. Lasers 48 0401011

[4] Gieseler J, Gomez-Solano J R, Magazzù A, Pérez Castillo I, Pérez García L, Gironella-Torrent M, Viader-Godoy X, Ritort F, Pesce G, Arzola A V, Volke-Sepúlveda K, Volpe G 2021 Adv. Opt. Photonics 13 74

[5] Yu S L, Lu J S, Ginis V, Kheifets S, Lim S W D, Qiu M, Gu T, Hu J J, Capasso F 2021 Optica 8 409

[6] Xu X H, Gao W Y, Li T Y, Shao T H, Li X Y, Zhou Y, Gao G Z, Wang G X, Yan S H, Wang S M, Yao B L 2024 Acta Opt. Sin. 44 0500001

[7] Yang J H, Deng R P, Wang X Y, Zhang Y Q, Yuan X C, Min C J 2024 Chin. J. Lasers 51 62

[8] Jia Q, Lyu W, Yan W, Tang W, Lu J, Qiu M 2023 Photonics Insights 2 R05-1

[9] Liu H J, Liu Y F, Gu F X 2024 Acta Phys. Sin. 73 104207

[10] Gu Z Q, Zhu R L, Shen T C, Dou L, Liu H J, Liu Y F, Liu X, Liu J, Zhuang S L, Gu F X 2023 Nat. Commun. 14 7663

[11] Zhang Y Z, Liu H J, Zhu R L, Liu Y F, Gu F X 2024 Chinese Journal of Lasers 51 1507403

[12] Shi Z X, Shen T C, Dou L, Gu Z Q, Zhu R L, Dong X Y, Gu F X 2024 Laser. Photonics. Rev. 18 2400384

[13] Zhu R L, Shen T C, Gu Z Q, Shi Z X, Dou L, Liu Y F, Zhuang S L, Gu F X 2024 ACS Nano 18 23232

[14] Gu Z Q, Dou L, Linghu S Y, Zhu R L, Gu F X 2024 Phys. Rev. Appl. 22 054066

[15] Song J K, Kim M S, Yoo S, Koo J H, Kim D H 2021 Nano Res. 14 2919

[16] Tan W S, Zhou J Z, Huang S, Sheng J, Xu J L 2016 Infrared and Laser Engineering 45 67

[17] Tang F, Pan D, Yu F, Huang K J, Hu Y L, Wu D, Li J W 2024 Chin. J. Lasers 51 1202401

[18] Bian P, Hu Z Y, An R, Tian Z N, Liu X Q, Chen Q D 2024 Laser Photonics Rev. 18 2300957

[19] Wang Y X, Liao C R, Zou M Q, Bao W J, Liu D J, Zhang L, Wang Y P 2024 Chin. J. Lasers 51 1202409

[20] Lee J, Kim J, Lee B J, Lee J, Lee H W, Hong M H, Park H H, Shim D Il, Cho H H, Kwon K H 2018 Thin Solid Films 660 715

[21] Tang T T, Wang Z H 2010 The Science of Micro- and Nano-fabrication (Beijing: Publishing House of Electronics Industry) p312

[22] Xing A, Gao Y, Yin J G, Ren G J, Liu H T, Ma M J 2010 Appl. Surf. Sci. 256 6133

[23] Kim S H, Hwang G S, Koo D, Seo D H, Kwon Y P, Lee H, Park H, Jeon E C, Kim J Y 2022 Nano Res. 15 7476

[24] Li T Y, Kingsley-Smith J J, Hu Y H, Xu X H, Yan S H, Wang S M, Yao B L, Wang Z L, Zhu S N 2023 Opt. Lett. 48 255

[25] Li T Y, Xu H H, Panmai M, Shao T H, Gao G Z, Xu F, Hu G W, Wang S N, Wang Z L, Zhu S N 2024 Ultrafast Sci. 4 0074

[26] Li T Y, Liu M J, Hou J H, Yang X, Wang S B, Wang S M, Zhu S N, Tsai D P, Wang Z L 2024 Chip 3 100109

[27] Guo J K, Sandaruwan W D N, Li J W, Ling J Z, Yuan Y, Liu X, Li Q, Wang X R 2024 Micromachines 15 337

[28] Liang Z S, Zhang B L, Yi S H, Sun K Y, Pei G H, Shang Y, Liu X Y, Ren S X, Liu P F, Zhao J J 2024 Nano Mater. Sci (In press

[29] Cheng Q L, Lu X Q, Tai Y H, Luo T T, Yang R H 2024 ACS Biomater. Sci. Eng. 10 5562

[30] Hou J Y, Liu H T, Huang L T, Wu S B, Zhang Z L 2024 Chem. Eng. J. 498 155135